Ratcheting Motion of Liquid Drops on Gradient Surfaces†

Susan Daniel, Sanjoy Sircar,‡ Jill Gliem, and Manoj K. Chaudhury*

Department of Chemical Engineering, Lehigh University, Bethlehem, Pennsylvania 18015

Received November 25, 2003. In Final Form: February 20, 2004

The motions of liquid drops of various surface tensions and viscosities were investigated on a solid substrate possessing a gradient of wettability. A drop of any size moves spontaneously on such a surface when the contact angle hysteresis is negligible; but it has to be larger than a critical size in order to move on a hysteretic surface. The hysteresis can, however, be reduced or eliminated with vibration that allows the drop to sample various metastable states, thereby setting it to the path of global energy minima. Significant amplification of velocity is observed with the frequency of forcing vibration matching the natural harmonics of drop oscillation. It is suggested that the main cause for velocity amplification is related to resonant shape fluctuation, which can be illustrated by periodically deforming and relaxing the drop at low frequencies.

Introduction

It is well-known[1−14] that a liquid drop placed on a chemically heterogeneous surface moves toward the region of higher wettability in order to minimize the interfacial free energy. The drop attains a steady velocity as soon as the driving force due to the wettability gradient is compensated by the viscous drag force. Since the motive force increases with the area and the drag force with the perimeter of contact, the steady-state velocity of the drop (expressed in terms of capillary number, *Ca*) increases linearly[1,2,12] with its base radius (*R*) as

$$Ca = \alpha R\left(\frac{\mathrm{d}(\cos\theta)}{\mathrm{d}x}\right) \qquad (1)$$

here $Ca = V\eta/\gamma$; V, η, and γ being the velocity, viscosity, and surface tension of the drop, and θ is the position-dependent contact angle. The coefficient α is a constant, provided that the drag forces at and near the contact line scale only with the bulk viscosity.[15] While, according to eq 1, liquid drops of all sizes should spontaneously migrate toward the region of higher wettability, in practice the drops have to be larger than a critical value before any such movement occurs.[6,12] The existence of such a critical radius is precisely due to wetting hysteresis, which manifests as a yield force at the three-phase contact line. The situation can be understood by considering that the contact angles of a liquid on a real surface are bounded by two extreme (advancing and receding) values. For a drop to move, its angle in the advancing edge must be smaller than that in the receding edge—a condition that is assured with hysteresis-free gradient surfaces but not necessarily with nonideal surfaces.[6,12]

The combination of the wettability gradient and local hysteresis, however, creates an interesting scenario when the drop is subjected to a periodic force. Like a conventional ratchet, the periodic force is rectified by the asymmetric hysteresis[12] that causes the drop to drift along the direction of higher wettability. The speed of the drop increases linearly with the amplitude of vibration but nonlinearly with both the frequency and drop radius. It is shown here that the origin of these nonlinearities is due to the resonant shape fluctuation in the drop that occurs when the vibration frequency approaches its natural spherical harmonics.

Results and Discussions

Migration of Liquid Drops on Gradient Surface in the Absence of Vibration. *Effects of Surface Tension and Viscosity***.** To appreciate the relationship between drop speed and hysteresis, we investigated the motion of liquid drops of various surface tensions and viscosities on a gradient surface that was prepared using a previously published method of diffusion-controlled silanization of a silicon wafer (see Experimental Section for the details of the procedure). The test liquids were dipropylene glycol, ethylene glycol, formamide, water, and acetonitrile having capillary velocities (ratio of surface tension to viscosity) of 0.4, 2.9, 17.9, 80.7, 83.5 m/s, respectively. Drops of these liquids of sizes ranging from ca. 0.5 to 2.5 mm were placed on the less wettable part of the gradient surface, and their migrations toward the higher energy side were investigated with a camera capable of recording images in the range of 30−2000 fps. Since the gradient of the viscous stress in most parts of the drop is very small except near the contact lines for low capillary number flows, the shapes of the moving drops on the gradient surfaces are those of hemispherical caps. Specifically, as argued by Greenspan[1], the gradient of local curvature (ξ_{xxx}) of the drop that dictates the driving force is related to the capillary number (*Ca*) and the local height (ξ) of the drop as $\xi_{xxx} \approx Ca/\xi^2$.

* To whom correspondence should be addressed.

† Parts of this paper were presented at the 2002 National ACS Meeting and at a 2003 ACS Symposium honoring D. Allara and R. Nuzzo.

‡ Current address: Department of Chemical Engineering, Massachusetts Institute of Technology, Cambridge, MA.

(1) Greenspan, H. P. *J. Fluid Mech.* **1978**, *84*, 125.
(2) Brochard, F. *Langmuir* **1989**, *5*, 432.
(3) Raphael, E. *C. R. Acad. Sci. Paris Ser. II* **1988**, *306*, 751.
(4) Carter, S. B. *Nature* **1967**, *213*, 256.
(5) Ondarcuhu, T.; Veyssie, M. *J. Phys. (Paris) II* **1988**, *1*, 75.
(6) Chaudhury, M. K.; Whitesides, G. M. *Science* **1992**, *256*, 1539.
(7) Ichimura, K.; Oh, S.-K.; Nakagawa, M. *Science* **2000**, *288*, 1624.
(8) Daniel, S.; Chaudhury, M. K.; Chen, J. C. *Science* **2001**, *291*, 633.
(9) Bain, C. D.; Burnett-Hall, G. D.; Montgomerie, R. R. *Nature (London)* **1994**, *372*, 414.
(10) Domingues Dos Santos, F.; Ondarcuhu, T. *Phys. Rev. Lett.* **1995**, *75*, 2972.
(11) Lee, S.-W.; Laibinis, P. E. *J. Am. Chem. Soc.* **2000**, *122*, 5395.
(12) Daniel, S.; Chaudhury, M. K. *Langmuir* **2002**, *18*, 9.
(13) Suda, H.; Yamada, S. *Langmuir* **2003**, *19*, 3.
(14) Choi, S.-H.; Zhang-Newby, B.-m. *Langmuir* **2003**, *19*, 18.
(15) Magnitude of α depends on the mechanism of the relaxation of stress singularity at the three-phase contact line. See refs 1−3 for more details.

10.1021/la036221a CCC: $27.50 © 2004 American Chemical Society
Published on Web 04/13/2004

For low capillary number cases (which, in our experiments, is less than 0.002), ξ_{xxx} is negligible (i.e., drop is a hemisphere) for most parts except very close to the contact lines, which is unresolvable within the limit of our optical techniques.

As shown first by Brochard[2] and discussed further in ref 12, the dynamic contact angle of the moving drop is, to a good approximation, equal to the Young's contact angle in the middle of the drop base.[16] Thus, the measurement of the dynamic angle on different locations on the gradient surface yields a good estimate of the wettability gradient (d(cos θ/dx)), whereas a frame by frame analysis of the drop position from the video-recorded images yields the speed of drop migration. As expected, the drop velocity increases with γ_l, R, and d(cos θ)/dx but decreases with the liquid viscosity, η. When the velocity and the radius of a liquid drop are nondimensionalized with capillary velocity ($V^* = \gamma/\eta$) and wettability gradient (d(cos θ/dx)) respectively, a linear correlation is observed between these variables for each liquid, in conformity with eq 1. An interesting point to note here is that these $Ca-R^*$ lines (here $R^* = R$(d(cos θ)/dx))are fairly parallel to each other even though the liquids are of different chemical compositions and the Reynolds number varies from 0.01 to 150. This implies that the frictional resistance of the moving contact line scales with the bulk viscosity of the liquid and that this resistance is considerably larger than the inertial forces even with such inviscid liquid as acetonitrile (Re $\approx$ 150). Another important point to note here is that for each liquid a threshold radius must be overcome for drop migration to occur. As pointed out earlier, this is a manifestation of the wetting hysteresis, i.e., the larger the hysteresis the larger the intercept on the radius axis.

This threshold radius can be calculated by balancing the Young's driving force due to the wettability gradient and the yield force due to hysteresis, resulting in the following equation[12]

$$\cos\theta_a - \cos\theta_r = \frac{\pi R}{2}\left(\frac{\mathrm{d}(\cos\theta)}{\mathrm{d}x}\right) \qquad (2)$$

Equation 2 yields the hysteresis ($\cos\theta_a - \cos\theta_r$) of acetonitrile, formamide, and water as 0.01, 0.21, and 0.27, which agree well with the values (acetonitrile 0.01, formamide 0.18, and water 0.27) obtained from dynamically advancing and receding the contact lines on the gradient surfaces. Large discrepancies are, however, observed with more viscous liquids as ethylene glycol (0.06 vs 0.1) and dipropylene glycol (0.01 vs 0.13), for which viscous bending of the drop shape near the contact lines is large enough to interfere with the measurements of true hysteresis. A related important point, as revealed from the linearity between Ca and R^*, is that the true hysteresis (i.e., that obtained from the intercept on the R^* axis) of each of these liquids is virtually independent of the velocity of drop migration as well as its position on the gradient surface.

Movements of Liquid Drops on Gradient Surfaces with Vibration. Recently, it has been demonstrated by several authors[17−19] that contact angle hysteresis of a liquid drop on a solid surface can be mitigated by supplying vibration energy to the drop. Inspired by these findings, we recently conducted a study in which a liquid drop on a gradient surface was subjected to an in-plane vibration with a square wave function that enhanced the velocity of drop beyond what is typically observed in the absence of vibration.[12] Here, we extend these studies with liquids of various surface tension and viscosity as well as by systematically controlling the amplitude and frequency of a sinusoidal vibration. As reported earlier, we find that many small drops, the motilities of which are arrested by hysteresis, move with appreciable speeds when vibrated. Furthermore, the larger drops that move sluggishly in the absence of vibration move even faster in its presence. However, unlike the linear correlation between the speed and radius seen with the nonvibrating drops (Figure 1), the speeds of the vibrating drops at first increase with size, but then a downward trend is observed for large size drops (Figure 3).

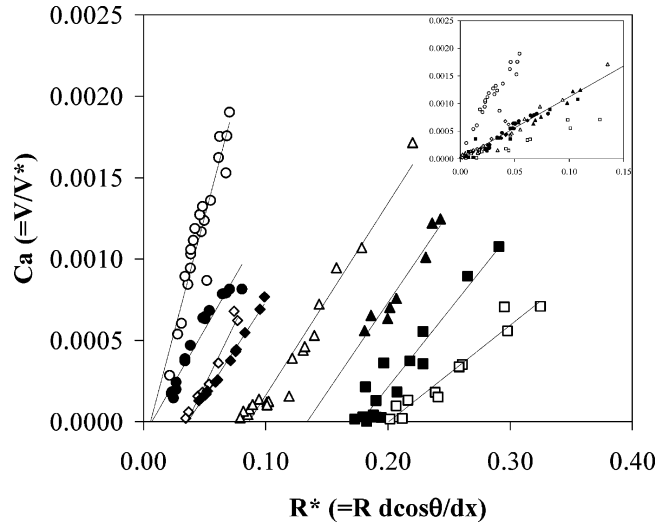

Figure 1. Nondimensionalized velocities of liquid drops on a gradient surface as a function of drop radius. Each liquid can be identified from the symbol(s) within the parenthesis as ethylene glycol (◆, ◇), dipropylene glycol (○), formamide (▲, △), water (■, □), and acetonitrile (●). Different symbols used for some of the liquids indicate that the experiments performed with these liquids on different surfaces are not exactly reproduced due to slight differences in contact angle hysteresis. In the inset, all the $Ca-R^*$ lines are shifted parallel to the R^* axis so that they all pass through the origin. The majority of the data obtained for all the liquids fall on a straight line (shown by the linearly regressed solid line), except those for dipropylene glycol.

An additional observation is that the vibration is most effective with liquids displaying a significant contact angle hysteresis, e.g., ethylene glycol, water, and formamide, but not with liquids exhibiting negligible hysteresis, i.e., acetonitrile and dipropylene glycol. These results illustrate the principle of half-wave rectification of mechanical pulses, mediated by the local asymmetry of contact angle hysteresis. A vibration that causes a net oscillation of the drop with its center of mass moving parallel to the vibrating surface allows the contact line to explore all possible energy states that separate the advancing and receding angles. As the drop identifies the globally minimal energy states in the spatial coordinate, hysteresis is effectively mitigated and the drop moves by experiencing the surface energy gradient that is otherwise obscured by hysteresis. This scenario may be mechanistically understood by considering the cross-section of a vibrating liquid drop, the advancing and receding edges of which are

(16) For a drop moving on a surface with minimum expansion of its base radius, the uncompensated Young's force on the two edges must be same, i.e., $\gamma_l(\cos\theta_a - \cos\theta) = \gamma_l(\cos\theta - \cos\theta_r)$, which leads to $\cos\theta = (\cos\theta_a + \cos\theta_r)/2$. As demonstrated by the authors of refs 17−19, the cosine average of the advancing and receding angles is also very close to the Young's equilibrium angles.

(17) Smith, T.; Lindberg, G. *J. Colloid Interface Sci.* **1978**, *66*, 363.
(18) Andrieu, C.; Sykes, C.; Brochard, F. *Langmuir* **1994**, *10*, 2077.
(19) Decker, E. L.; Garoff, S. *Langmuir* **1996**, *12*, 2100.

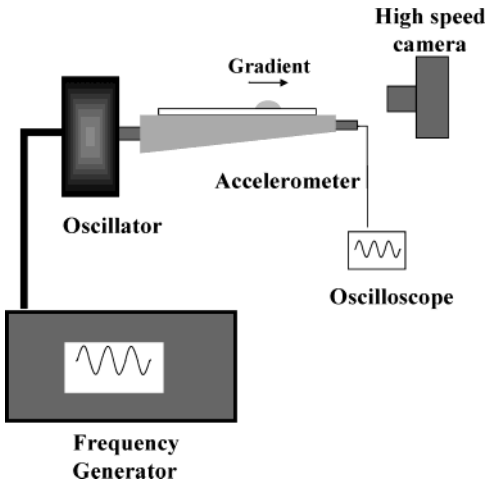

Figure 2. Schematics of the apparatus used to vibrate the liquid drops on a gradient surface supported on a silicon wafer. The wafer is attached to a rigid aluminum support, which minimizes oscillation in the vertical direction. The aluminum plate is connected to an oscillator that is driven by a frequency generator. The accelerometer measures the acceleration of the plate, and the high-speed camera is used to examine the motion of the drops.

located at points B and A, respectively (Figure 4a). If the velocity of the vibrating plate is $V_o \sin(2\pi\omega t)$ (V_o = amplitude, ω = frequency), then the relative velocity between the contact line and the plate can be expressed by balancing the capillary, viscous, and inertial forces that the drop experiences. By considering that the displacement[20] of a plane within the drop parallel to the drop−water interface follows eq 3

$$u = u_o \exp\left(-\frac{z}{e}\right)\cos\left(2\pi\omega t - \frac{z}{e}\right) \tag{3}$$

the resultant velocity of the drop during the first and second half of the oscillation cycles can be expressed as follows

$$\frac{dx}{dt} - V_o \sin 2\pi\omega t - \frac{\alpha V^*}{2}(\cos\theta_{aB} - \cos\theta_{rA}) + \frac{\rho\omega^2 u_o}{\eta R}\int_V \exp\left(-\frac{z}{e}\right)\cos\left(2\pi\omega t - \frac{z}{e}\right)dV = 0$$
$$0 \le t \le 1/2\omega \tag{4}$$

and

$$\frac{dx}{dt} - V_o \sin 2\pi\omega t - \frac{\alpha V^*}{2}(\cos\theta_{rB} - \cos\theta_{aA}) + \frac{\rho\omega^2 u_o}{\eta R}\int_V \exp\left(-\frac{z}{e}\right)\cos\left(2\pi\omega t - \frac{z}{e}\right)dV = 0$$
$$1/2\omega \le t \le 1/\omega \tag{5}$$

here u_o is the amplitude of the plate, V is the drop volume, ρ is the density, z is the vertical distance, e is the Stokes length $\sqrt{\upsilon/\omega}$, υ is the kinematic viscosity. Net displacement of the drop in each complete cycle is obtained by integrating eqs 4 and 5 with respect to time and then adding them. However, time integrals of the third and fourth terms in a full cycle vanish, so that the net displacement of the drop in each vibration cycle is

$$x = \frac{\alpha V^*}{4\omega}[(\cos\theta_{rB} + \cos\theta_{aB}) - (\cos\theta_{aA} + \cos\theta_{rA})] \tag{6}$$

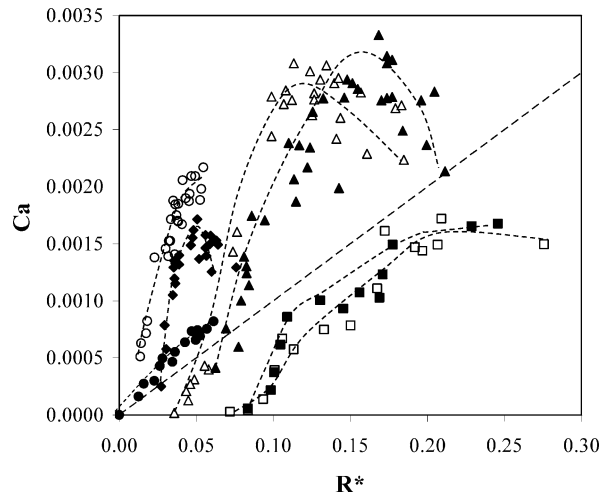

Figure 3. Velocities of liquid drops on a gradient surface as a function of drop radius at a frequency and amplitude of vibration of 100 Hz and 3.1×10^{-4} m, respectively. Each liquid is denoted by the symbol within the parentheses as ethylene glycol (◆), dipropylene glycol (○), formamide (▲, △), water (■, □), and acetonitrile (●). The dashed line is that obtained from the inset of Figure 1.

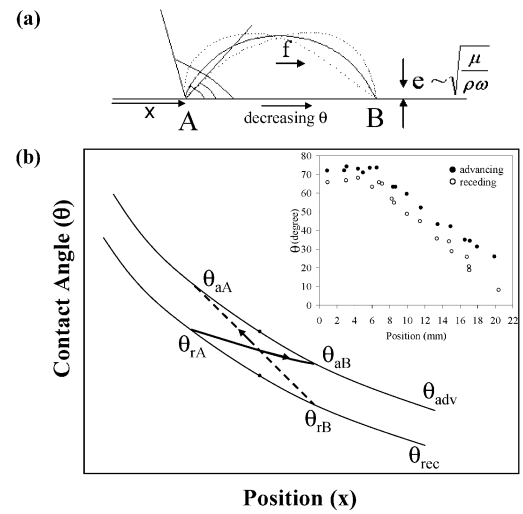

Figure 4. (a) Cross-section of a vibrating drop, where the undisturbed profile of the drop is shown by the solid line and that of the vibrating profile by the dotted line. f is inertial force on the drop due to the vibration. e is the Stokes length that corresponds to the region of the liquid drop under the influence of viscous forces. The region above it is primarily under the influence of inertial force. (b) General patterns of advancing (θ_a) and receding (θ_r) angles of liquids on a gradient surface, with the real values of ethylene glycol shown in the inset. The front edge (B) of a liquid drop is characterized by the advancing angle θ_{aB}, whereas the rear edge (A) is characterized by the receding angle θ_{rA}. If $\theta_{aB} \ge \theta_{rA}$, the drop does not move. However, if the drop is subjected to a periodic force, it gets rectified by asymmetric hysteresis since $\cos\theta_{rB} - \cos\theta_{aA} > \cos\theta_{aB} - \cos\theta_{rA}$.

Now, recalling that the average of the cosines of advancing and receding contact angles is the same as the cosine of the equilibrium contact angle and expressing this angle as

$$\cos\theta_B = \cos\theta_A + 2\frac{d(\cos\theta)}{dx}R \tag{7}$$

we have the velocity ($x\omega$) of the drop in each cycle of vibration, which is the same as that given in eq 1.

The above exercise suggests that vibration adds nothing to the drop on a hysteresis-free gradient surface, as is the case with acetonitrile and dipropylene glycol. For other surfaces, it should merely eliminate hysteresis. Even though the first proposition conforms well to experimental observation, a significant amplification of velocity occurs in addition to rectification for hysteretic surfaces. There is evidence to suggest that this velocity augmentation is due to the fluctuation of the liquid drop about its equilibrium shape as discussed below.

Resonant Shape Fluctuation. For a drop oscillating on a gradient surface with forcing amplitude A and frequency ω, the rectified velocity should be proportional to $A\omega$. Experimentally, while it is found that the velocity increases linearly with amplitude, it varies nonlinearly with frequency either at a given inertial force ($A\omega^2 =$ constant) or at a constant amplitude ($A =$ constant). Here we focus our attention on the data corresponding to constant amplitude, which exhibit two peaks—one in the range of 100−150 Hz and the other in the range of 250−350 Hz.

A closer look at these frequencies indicate that they are similar to the first and second spherical harmonics of a freely oscillating liquid drop which can be expressed according to Rayleigh's equation as follows[21,22]

$$\omega = \sqrt{\frac{\gamma}{3\pi m}(n)(n-1)(n+2)} \qquad (8)$$

here m is the mass of the drop and n is an integral value of 2 or higher. The term $(\gamma/m)^{1/2}$ in eq 8 is similar to the vibration frequency of a mass attached to a spring with the surface tension term replacing the spring constant.

The natural frequencies of vibration of sessile or pendant liquid drops have been studied by several authors[23−30] using both computational and experimental methods. The motivation for those studies stems from the relevance of the oscillation of supported drops to various technological processes, such as liquid−liquid extraction, synthesis of ceramic powders, crystal growth in microgravity, as well as the measurement of dynamic surface tension. In view of those developments,[23−30] Equation 8 is considerably approximate in that it does not account for the effects of viscous damping and the associated nonlinearities as well as the constraints the drop experience while in contact with a solid surface. The latter issue was brought about by Strani and Sabetta,[30] who pointed out that a drop in partial contact with a surface has an extra vibration mode at a very low frequency that is absent in the case of free drops, whereas the higher modes of vibration in two cases are similar to each other. Our current problem is even more unique in the sense that the oscillatory inertial force is applied to the drop parallel to the surface of contact, where the periodic motion of the drop alters its resonance shapes. In the absence of a proper hydrodynamic analysis of a drop vibrating parallel to a substrate, we adopt here a qualitative approach. Specifically, we conducted a test study in which the natural resonance modes of sessile drops of water of various sizes were determined by vibrating them laterally on a uniformly hydrophobic surface at a low amplitude but at various frequencies. The resonance modes were discerned from the characteristic ghost images (Figure 6) of the oscillating drops, which indeed vary inversely with the square root of the drop mass as predicted by eq 8.

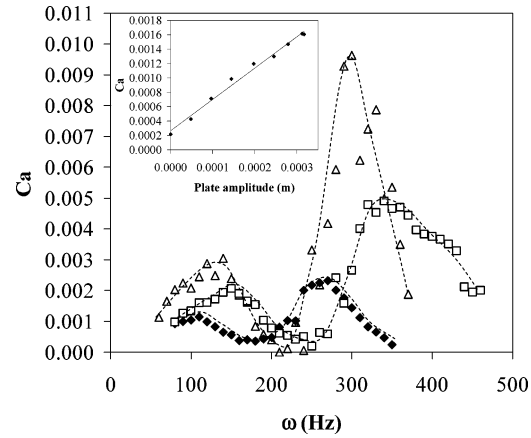

Figure 5. Velocity of liquid drop increases linearly with amplitude (inset shows the typical data of ethylene glycol, $\omega = 100$ Hz, mass of liquid drop $= 2.3 \times 10^{-6}$ kg) but nonlinearly with the frequency of vibration. Frequency-dependent data are shown for three liquids, ethylene glycol (●), formamide (△), and water (□), which exhibit significant hysteresis of contact angle and thus a significant amount of amplified rectification. These velocity data were initially collected at constant inertial force ($A\omega^2 = 3.1$ m/s^2). With appropriate scaling (see text for details), all data are transformed to a constant amplitude of 3.1×10^{-4} m.

To check if the amplification of velocity of the liquid drops corresponds to the natural harmonics obtained above, we also examined the frequency-dependent velocity responses of the water drop of three different sizes on a given gradient surface. As predicted, the frequencies corresponding to maximum velocities decrease with the drop size (Figure 7), with the peak positions corresponding to the first and second natural harmonics of water drops (Figure 6). These results encouraged us to consider whether the velocity peaks for other liquids (Figure 5) correspond to their natural harmonics as well. To test this idea, all the velocity−frequency data of Figure 5 were nondimensionalized by dividing the forcing frequency with the natural frequency of the drop $\omega^* = \sqrt{\gamma/m}$. This application shifted all the peaks of Figure 5 in such a way that the frequencies corresponding to the first and second velocity maxima for all the liquids now nearly coincide. Next, we tried to transform the velocity−radius data of Figure 3 to a frequency axis by assigning a characteristic frequency to every radius using the following equation $\omega^* = \sqrt{3\gamma/\rho\pi h^2(3R-h)}$, where R is the radius of the drop and h is the height of the drop at its apex. As shown in Figure 8, these data also collapse near the lower ranges of the frequency responses for each liquid.

(20) This solution of the momentum transport equation is analogous to a heat-transfer problem with oscillating surface temperature as shown in Carslaw, H. S.; Jaeger, J. C. *Conduction of Heat in Solids*, 2nd ed.; Clarendon Press: Oxford, 1959. It is assumed that the Stokes length (e) is considerably smaller than the size of the drop. Another approximate solution would be to treat the drop above the thin boundary layer following a rigid body dynamics, in which case the displacement of the mass would follow an equation $\approx x_0 \sin(\omega t - \phi)$, ϕ being the phase shift. Time-average displacement of the drop in a full cycle is still zero however.

(21) Lamb, H. *Hydrodynamics*; Cambridge University Press: Cambridge, U.K., 1932.
(22) Chandrasekhar, S. *Hydrodynamic and Hydromagnetic Stability*; Dover: Mineola, NY, 1961.
(23) Kalechits, V. I.; Nakhutin, I. E.; Poluektov, P. P. *Sov. Phys. Technol. Phys.* **1985**, *29*, 934.
(24) Smithwick, R. W.; Boulet, J. A. M. *J. Colloid Interface Sci.* **1989**, *130*, 588.
(25) Kalechits, V. I.; Nakhutin, I. E.; Poluektov, P. P.; Rubezhnyi, Yu. G.; Chistyakov, V. A. *Sov. Phys. Technol. Phys.* **1979**, *5*, 496.
(26) Yoshiyasu, N.; Matsuda, K.; Takaki, R. *J. Phys. Soc. Jpn.* **1996**, *65*, 7.
(27) Basaran, O. A.; DePaoli, D. W. *Phys. Fluids* **1994**, *6*, 2923.
(28) Wilkes, E. D.; Basaran, O. A. *Phys. Fluids* **1997**, *9*, 1512.
(29) Rodot, H.; Bisch, C.; Lasek, A. *Acta Astronautica* **1979**, *6*, 1083.
(30) Strani, M.; Sabetta, F. *J. Fluid Mech.* **1984**, *141*, 233.

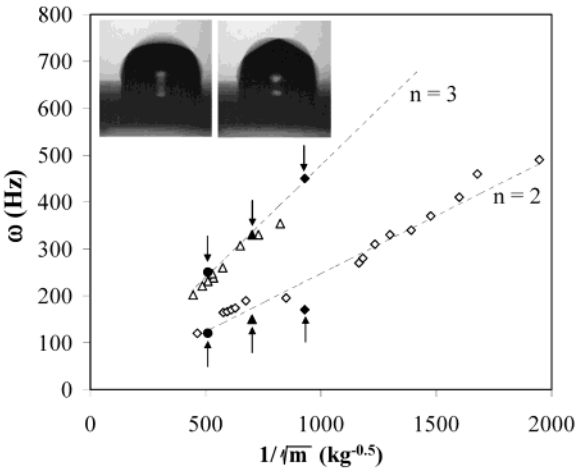

Figure 6. Resonance frequencies of a drop of water as a function of its mass but at a constant maximum acceleration of 0.64 m/s^2. We focused on the first and second resonant modes as shown in the inset, which can be seen as ghost images in an ordinary video camera at 30 fps. The dashed lines correspond to the resonant modes of the first and second harmonics according to eq 8 for $n = 2$ and 3. The data marked with arrows are from the figures reported in Figure 7, where ◆, ▲, and ● correspond to water drops of mass 1.16×10^{-6}, 2.04×10^{-6}, and 3.86×10^{-6} kg, respectively.

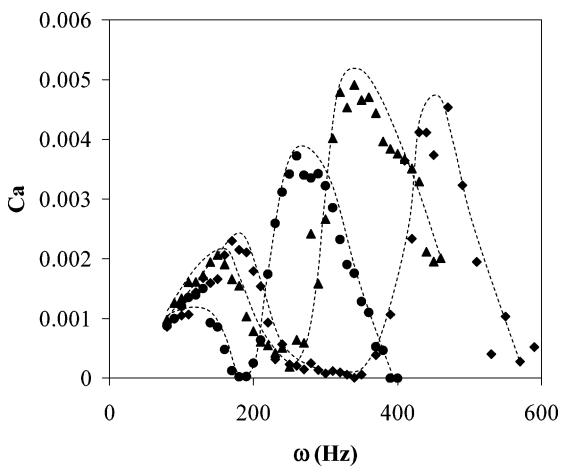

Figure 7. Velocity of water drops on a surface as a function of vibration frequency and drop mass. ◆, ▲, and ● correspond to 1.16×10^{-6}, 2.04×10^{-6}, and 3.86×10^{-6} kg, respectively. As the mass of the water drop increases, the first and second harmonics are shifted to the left as predicted by eq 8. The peak frequencies are close to the correlation reported in Figure 6.

Such a satisfactory collapse of data on a single master curve for each liquid with the velocity peaks corresponding to the first and second resonance modes of the water drops begs answer to the question whether it is the resonance energy transfer to the contact line that is responsible for velocity amplification or a geometric effect. Partial answer to this question is obtained from a slightly different experiment as discussed below.

Direct Evidence of Velocity Amplification via Shape Fluctuation. That the shape fluctuation, in the absence of the lateral oscillation of the center of mass, is sufficient to produce a ratcheting motion has been demonstrated by Silberzan et al.[31−33] These authors induced a shape fluctuation in a drop confined between two surfaces having saw-tooth patterns of roughness by alternating electrical fields. Assisted by electrowetting and shape fluctuation, the three-phase contact line undergoes successive stages of pinning and depinning actions, thereby causing a net motion of the drop on such surfaces. A similar demonstration of drop motion can be made on a gradient surface with asymmetric hysteresis by bringing the drop into contact with a hydrophobic surface and vibrating the latter at a low frequency (1−10 Hz, Figure 9). Here, as the drop is squeezed, the contact line corresponding to higher wettability moves forward while the rear end remains pinned. Just the opposite scenario emerges during the reverse process, resulting in a net forward displacement of the drop in each cycle, which multiplied by the frequency of oscillation gives the resulting velocity of the drop motion. These results as well those of Silberzan et al.[31−33] suggest that the geometric shape fluctuation is sufficient to induce motion to a liquid drop on an asymmetric surface and that the results of Figure 8 can be understood in the same light. This, however, does not preclude the notion that the enhancement of velocity is also impacted by the fluctuation-induced depinning of contact line from metastable states, which was offered earlier as an explanation for the vibration-assisted reduction of contact angle hysteresis[17−19] on some low-energy surfaces.

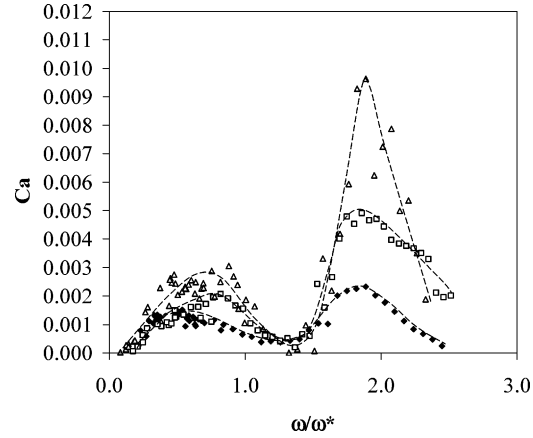

Figure 8. Frequency-dependent velocity of the three liquid drops (water (□), ethylene glycol (◆), and formamide (△)) as reported in Figure 5 are shown here after dividing the forcing frequency with $\omega^* = (\gamma/m)^{1/2}$. The data reported in Figure 3 are also transformed to the frequency plane by transforming the radius to frequency as discussed in the text.

Switching, rectification, and amplification are some of the basic operations that are cornerstones to the controls of dynamic systems. Control of fluid flow in batch fluidic operations is no exception. A crude demonstration of some of these concepts on a surface patterned with intersecting gradients is illustrated in Figure 10. Practical realizations of devices based on these concepts, however, must wait until remote mechanism(s) of drop shape fluctuation are perfected. Various mechanisms based on magnetic (Whitesides, G. M. Personal discussion) and electrical (Silberzan, P. Personal discussion) inductions as well as localized transfer of acoustic energy could be envisaged for this purpose. In some applications, however, this external field is unnecessary, as is the case with multiple drops coalescing on a gradient surface (see below).

(31) Sandre, O.; Garre-Talini, L.; Ajdari, A.; Prost, J.; Silberzan, P. *Phys. Rev. E* **1999**, *60*, 2964.

(32) Buguin, A.; Talini, L.; Silberzan, P. *Appl. Phys. A* **2002**, *75*, 207.

(33) Silberzan et al. (Silberzan, personal communication, Sept. 2003) induced an amplification of velocity to water drops by matching the forcing frequency of oscillation of the drop to its natural frequency. See also: Foulillet, Y.; Jeanson, H.; Chartier, I.; Buguin, A.; Silberzan, P. Congres SHF "Microfluidique", Toulouse, Dec 2002.

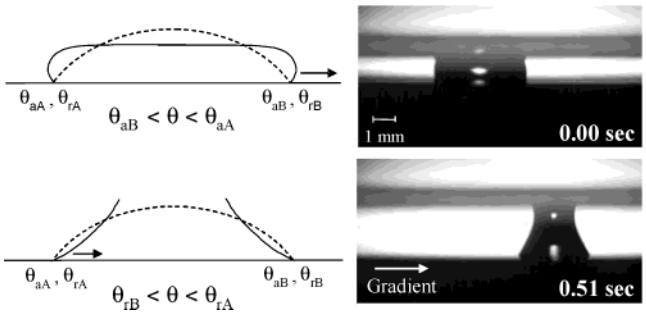

Figure 9. Movement of a water drop confined between a gradient (lower) and a hydrophobic (upper) surface. The upper surface is vibrated with a frequency of 1 Hz. As the drop is squeezed, its contact angle (θ) tends to be larger than both θ_{aA} and θ_{aB}. However, as $\theta_{aB} < \theta_{aA}$, the uncompensated force drives the contact line at B to move to the right before θ can reach θ_{aB}. Similarly, during the reverse stroke θ tends to be smaller than both θ_{rA} and θ_{rB}. However, as $\theta_{rB} < \theta_{rA}$, the contact line at A moves right before θ reaches θ_{rA}. The successive pinning and depinning of contact lines causes a net motion of the drop toward the more wettable portion of the gradient.

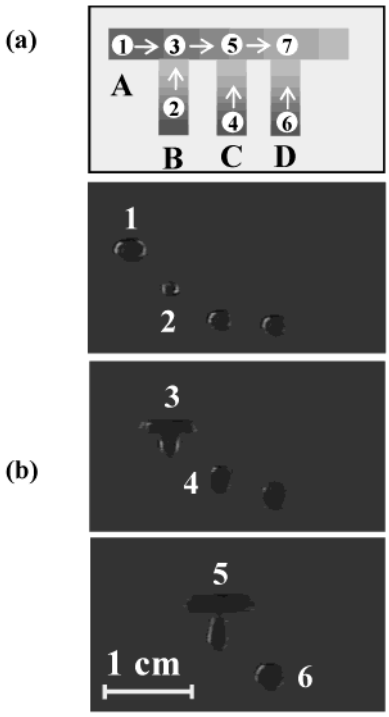

Figure 10. (a) Schematic of a fluidic device that operates on the principle of rectified drop motion described in Figure 9. The channel (1−7) has a surface energy gradient from left to right. The gradients of the other three channels are bottom up. When shape fluctuation is initiated, drop at 1 moves to the right and coalesces with the drop 2 moving upward at 3. The coalesced drop at 3 then moves right and coalesces with the drop at 4 moving upward. Finally, the coalesced drop at 5 merges with drop 6 at 7 (not shown in figure).

Rectification Due to Drop Coalescence. Zhao and Beysens[34] were first to report that when condensation occurs from a partially saturated atmosphere onto a heterogeneous surface, occasionally two or more drops coalesce with each other with the center of mass of the resultant drop moving toward the region of higher wettability.

This phenomenon is reminiscent of the shape fluctuation-driven rectified motion, which partially explains the previously reported high speeds (~1 m) of water drops obtained from the condensation[8] of steam on a gradient surface. Coalescence-induced rectified motion of water drops is illustrated in Figure 11, which shows that the center of mass of two coalesced drops moves toward the region of higher wettability. When multiple droplets undergo such coalescence, rather fast movement can be observed even with drops as small as 100 μm, which, in general, do not move without any external perturbations. In Figure 12 we present the typical velocities obtained from the impingement and simultaneous coalescence of multiple drops produced by exposing a gradient surface to a mist of water.

Here, keeping with the randomness of the coalescence process, a wide distribution of drop speed is observed, the

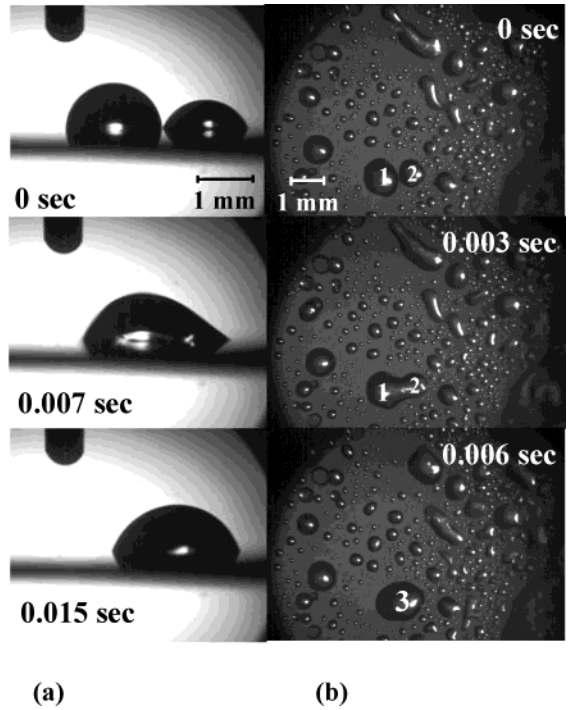

Figure 11. Coalescence-induced rectification of water drops on gradient surfaces. (a) Side views of the coalescence of two isolated drops of base radius ~0.9 and 0.8 mm. Figure 10b shows the sequences of coalescences of two drops 1 and 2 in the case of multiple drops impinging on a gradient surface. In all cases, the coalesced drops move toward the region of higher wettability.

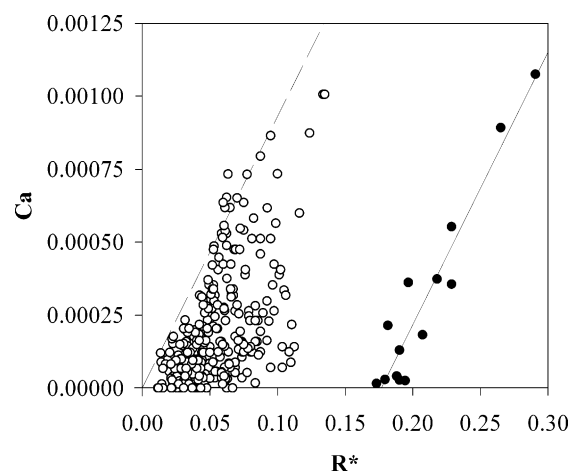

Figure 12. Coalescence-induced rectification of liquid drops on a gradient surface. Open symbols indicate the distribution of velocity of drops coalescing on the gradient surface showing an upper bound. The closed circles represent the velocities for drops on a similar surface without any rectification.

(34) Zhao, H.; Beysens, D. *Langmuir* **1995**, *11*, 627.

upper bound of which surprisingly falls on a straight line. The fact that this line passes through the origin with a slope that is the same as that obtained with water drops moving on similar surfaces in the absence of condensation indicates that the hysteresis is completely eliminated. Similar results, but with the slope of the $Ca-R^*$ line even higher than that presented in Figure 12, are observed with water drops produced from the condensation of steam on a gradient surface. These differences of drop velocities are related to various factors, the most important of which is the collision frequency of drops, which for condensation is much larger than the situation described here. The details of these results will be published separately.

Summary and Conclusions

These studies show that contact angle hysteresis, which is the major detriment to the motion of liquid drops on gradient surfaces, can also be used to rectify periodic pulses, thereby giving rise to a ratcheting motion. While both the amplitude and frequency of vibration affect the ratcheting motion, velocity increases linearly with amplitude but rather nonlinearly with frequency. Maximum velocities are obtained for each liquid when the forcing frequency matches the first and second spherical harmonics of the drop, suggesting that the ratcheting efficiency is at its maximum when the drop undergoes a resonant shape fluctuation. Shape-fluctuation-induced ratcheting action can also be simulated by periodically deforming and relaxing the drop on an asymmetric surface, which resembles one of the modes of locomotion of terrestrial animals[35,36] that results from the dynamic rectification of periodic muscular deformations via asymmetric interfacial friction. This shape-fluctuation-driven rectified motion takes place automatically when multiple drops coalesce on an asymmetric surface, the practical applications of which may be found in enhancing the efficiency of heat-transfer devices and heat pipes.

Experimental Section

General Information. The liquids used for the various experiments were acetonitrile, dipropylene glycol, ethylene glycol, formamide, and water. Acetonitrile (Fisher) was HPLC-grade and had a surface tension of 29 mN/m. Dipropylene glycol (Aldrich, 99%) had a surface tension of 35 mN/m. Formamide (Aldrich, 99+%) was spectrophotometric grade with a surface tension of 59 mN/m. Ethylene glycol (Sigma) had a surface tension of 47 mN/m. Water was purified with a Nanopure water purifier (Barnstead) with a surface tension of 72 mN/m. Decyltrichlorosilane, $Cl_3Si(CH_2)_8CH_3$, obtained from Gelest, was used to make the gradient surfaces. The silicon wafers (100) used in the studies of drop motion were obtained from Silicon Quest International. While studying the cooperating motion of water droplets in a mist, glass microscope slides (Corning, 3 in. ×1 in., plain) were used. Plasma oxidation was carried out in a Harrick Plasma Cleaner (model PDC-32G). The microsyringes used to measure contact angles and to deposit drops on surfaces were obtained from Gilmont Instruments. Contact angle measurements were carried out with a Rame Hart goniometer equipped with a digital camera (Redlake MotionPro, model 2000) connected to a PC. The mechanical oscillator used to induce vibration in the drops was from Pasco Scientific, model SF-9324, and equipped with a function generator (Agilent, model 33120A) and a power amplifier (Pasco Scientific, model CI-6552A). An accelerometer (PCB Piezotronics) was used to measure the acceleration of the substrate during the vibration experiments, which was connected to a oscilloscope obtained from Tektronix (model 2236). Drop motion was recorded using a high-speed camera (Redlake MotionPro, model 2000) capable of recording up to 2000 frames/s and/or a Sony CCD camera (model XC-75) equipped with a Nikon telescopic photolens (model SMZ-2T).

Preparation of Gradient Surfaces. Silicon wafers were cut into thin strips of approximately 5 cm × 2.5 cm and cleaned by soaking them in piranha solution (mixture of 30% H_2O_2 (50% solution) and 70% H_2SO_4) for 30 min. They were then copiously rinsed with and stored in distilled water before further use. The silicon strips were dried using ultra-high-purity N_2 gas (MG Industries) and treated with an oxygen plasma at 0.2 Torr for 45 s on the lowest setting in a Harrick Plasma Cleaner (model PDC-32G) immediately before the preparation of the gradient. An axial gradient of surface energy was prepared on the silicon substrate by diffusion-controlled silanization of decyltrichlorosilane. A 100% polyester thread, tightly stretched across a rigid frame, was soaked in pure silane. The thread was then positioned above (~2 mm) the edge of the silicon strip allowing silane to evaporate, diffuse, and react with the silicon ($Si/Si0_2$) surface. The edge of the wafer, which was closest to the silane source, became maximally hydrophobic, whereas the distant parts became progressively hydrophilic. To prepare good-quality surfaces, a low-humidity environment was an important requirement as it minimized the hydrolysis of the silane by atmospheric water. Atmospheric or adsorbed water is of particular concern as it competes with the surface silanols in reacting with the chlorosilanes. The following sets of conditions yielded results of satisfactory reproducibility. First, the relative humidity of the deposition chamber was maintained at <10% by flushing the deposition chamber (85 cm × 52 cm × 30 cm) with dry air produced by a Ballstone FTIR purge gas generator. Second, the air convection was minimized in order to prepare the gradient. This was accomplished by locally isolating the deposition components (silicon substrate, silane source, etc.) within the rigid glass frame while the silanization reaction was carried out inside the deposition chamber. A rather steep gradient (~1 cm length) could be prepared using decyltrichlorosilane as the source with the total reactive diffusion time of 2.5 min. All depositions were carried out at room temperature (~23 °C). Immediately following deposition, the wafer was placed inside a clean Petri dish and transferred to an oven at 60 °C for 15 min to instigate any loosely bound silane molecules to react fully with the surface. Prior to the experiments, the surface was washed with purified water and dried with high-purity N_2 in order to remove any residual silane or particles adhered to the surface. Surface energy gradients used to study the coalescence-induced rectification of water drop motion were also prepared using the method outlined above, except that the substrate used was not a silicon wafer but a glass microscope slide. The main reason for the change in substrate was due to constraints in the data collection. In this experiment, it was required that the substrate be transparent so that the camera could be positioned behind the slide to record the drop motion, to minimize its interference with the drop impingement, as well as to isolate the camera lens from the mist.

Studying Drop Motion Without Vibration. Drops of varying radii were placed on the less wettable part of the gradient using a microsyringe, and their motions toward the more wettable side were recorded using a Redlake MotionPro (model 2000) camera. The gradient usually is flatter near the edge and steeper in the middle of the silicon strip. Consequently, a drop deposited on the flatter part of the gradient moved slowly at first before entering into the linear region of the gradient where it moved steadily. This method of allowing the drop to move slowly in the beginning ensured the dissipation of gross disturbances resulting from the transfer of the drop to the surface from microsyringe. Video recording captured the entire motion of the drop profile as it moved along the gradient; however, the velocity was measured only in the linear portion of the gradient. To minimize the effects of extraneous vibration, the entire setup was placed on the top of a vibration isolation table (Micro-g, TMC).

Apparatus Used To Induce Vibration in Drops. Gradient surfaces were securely attached to a flat rigid aluminum platform with double-sided adhesive tape. The metal platform was clamped securely onto the stem of a mechanical oscillator (Pasco Scientific, model SF-9324). The latter was controlled by a waveform generator (Agilent, model 33120A) capable of generating various shaped waves in the frequency range of 0.001−100 kHz. The signal from the function generator was fed into a power amplifier (Pasco Scientific, model CI-6552A), which was then connected to the mechanical vibrator to drive the oscillations. The direction

(35) Keller, J. B.; Falkowitz, M. *J. Theor. Biol.* **1983**, *104*, 417.
(36) Mahadevan, L.; Daniel, S.; Chaudhury, M. K. *PNAS* **2004**, *101*, 23.

of vibration with respect to the plane of the substrate was controlled by adjusting the orientation of the oscillator. In- and out-of -plane vibration were monitored with an accelerometer (PCB Piezotronics) attached to the metal clamp. The accelerometer signal was fed to an oscilloscope (Tektronix, model 2236) for in-situ monitoring of vibration that was produced.

Studying Drop Motion With In−Plane Vibration. The motions of liquid drops on the gradient surfaces vibrated sinusoidally parallel to its plane were recorded with a high-speed camera (Redlake MotionPro, model 2000). The frequencies (60−590 Hz) and amplitudes were set on the function generator (Agilent, model 33120A). This oscillator maintains a constant inertial force during vibration. Nevertheless, data taken at different frequencies and/or inertial forces could be transformed to those corresponding to constant amplitude by using the relationship: $A_1\omega_1^2 = A_2\omega_2^2$. Experiments were carried out in the following order for each liquid: initially, velocities were measured as a function of the base radii of the drops which range from ca. 0.5 to 2 mm. At the conclusion of this experiment, data corresponding to in-plane vibration were taken at a constant plate amplitude (0.31 mm) and frequency (100 Hz) over a range of radii (0.3−2.5 mm). The second series of experiments were carried out for each liquid with a constant drop size but varying signal frequency from 60 to 590 Hz. In the third set of experiments, velocity was measured as a function of plate amplitude (0.05−0.32 mm) but keeping the drop size and frequency constant. Plate amplitude was determined by measuring the maximum displacement of the plate from its neutral position from their video-recorded images.

Measurements of Drop Velocities. A Redlake MotionPro high-speed camera (30−2000 fps) recorded the images of the drop as it moved on the surface. The frame rates used to record the images varied according to the speed of the drop, i.e., recording of the faster drop motion required fps ranging from 500 to 2000, whereas for the slower moving drops (highly viscous drops or very small drops), the recording frame rate was as low as 30 fps. The positions of both the advancing and receding drop edges were tracked with a Redlake Midas (version 2.0.5 r) motion analysis software, from which the average position of the center of the drop was estimated. All the dynamic contact angles and velocities were measured within the linear regions of the gradient as ascertained from contact angle measurements.

Measurement of the Natural Frequency of the Drop. Drops of water of various sizes were deposited onto a uniformly hydrophobic surface made with decyltrichlorosilane. The substrates were vibrated parallel to its plane beginning at a frequency of 80 Hz and gradually increasing it until a harmonic mode was observed. These modes were visually striking and easily recognizable from the ghost images captured with a low-speed camera (30fps).

Apparatus Used To Induce Shape Fluctuation in a Drop on a Gradient Surface. Shape fluctuation was induced in a water drop by periodically squeezing it between the gradient surface and a uniformly hydrophobic surface. In this circumstance, the gradient surface was attached to a metal clamp fastened to the oscillator so that sinusoidal plate oscillation occurred in the direction perpendicular to the substrate. A small water drop was placed on an axial gradient using a microsyringe, where it remained pinned due to contact angle hysteresis until deformation was initiated. A Redlake MotionPro (model 2000) camera recorded the profile of the drop at 250 fps as it moved down the gradient during deformation cycles. The frequency of drop deformation ranged from 1 to 20 Hz, and it was observed that drop speed varied linearly with both frequency and amplitude.

Fabrication of Drop Network on Silicon Chip and Induction of Drop Motion. A gradient channel network was fabricated on a small 2.5 cm × 5 cm rectangular silicon wafer strip as an extension of a method published in ref 6. The cleaned strip was first hydrophobized by exposing it to the vapor of decyltrichlorosilanes in air by placing a silane-soaked filter paper 2 mm above it for 22 min. After covering the hydrophobic substrate with an adhesive tape, the channel design was scored and the cut sections of the tape were selectively removed. After exposing the strip to an oxygen plasma for 45 s, the gradients in the channels were made sequentially in two-stage processes of diffusion-controlled silanization. First, the shorter channels, denoted by letters B, C, D in Figure 10, were exposed to the diffusing front of a decyltrichlorosilanes line source for 2 min, while channel A was covered with a cover slip to minimize exposure of this area to silane. In the next step, channels B, C, and D were covered with a glass cover slip and the gradient was formed in channel A. After the gradients were complete, the adhesive tape covering the hydrophobic areas was removed. After placing drops of water at the mouth of the channels, a hydrophobic glass plate was brought into contact with them and fixed at a given height. The substrate underwent sinusoidal oscillation (2 Hz) perpendicular to the substrate, thus squeezing and deforming the drops placed on the channels. The drop motions were recorded with a Sony Digital Handycam, model DCR-TRV130.

Apparatus Used To Create Mist Impingement on Gradient Surfaces. An air jet was oriented perpendicularly to a water stream, creating a mist of water drops, which was made to impinge on a glass slide possessing a gradient of decyltrichlorosilane. A microscope/camera system (1000 fps) recorded the drop motions continuously from the backside of the glass slide. Drop velocities were determined from the distance traveled by the drop between two successive recorded images. Drop radius was taken to be the average of the radius in each frame. The flux of the mist (~0.15 L/m^{2}s) to the surface was measured by orienting the mouth of an Erlenmeyer flask in front of the mist stream at approximately the same distance from the mist source and collecting the volume of liquid in time.

Measurement of Contact Angles. Contact angle measurements on the gradient surfaces were made with each of the test liquids: acetonitrile, dipropylene glycol, ethylene glycol, formamide, and water. A small drop was formed on the solid surface using a needle attached to the microsyringe. While the drop was in contact with the solid, additional liquid was slowly added to the drop, thus advancing the contact line. The receding angle was measured while slowly withdrawing liquid from the drop following the same procedure. The angles were measured from an instantaneous video picture as the contact line advanced or receded along the surface. The image was projected on a computer screen where graphic software was used to measure the angle between the tangent line at the three-phase contact line and the horizontal substrate. The position-dependent angles were measured axially along the gradient by moving the syringe's position down the length of the substrate, a millimeter or less at a time, and performing the above steps at each position. These measurements were carried out under ambient conditions. This method worked well for most liquids, except for the highly viscous liquid dipropylene glycol, where it was observed that the relaxation time for the contact line was much longer; thus, the values of the advancing and receding angles obtained in this way tended to be slightly larger or smaller than the true advancing and receding angles.

Measurement of the Dynamic Contact Angle. The dynamic contact angles as a function of position were measured from the video images of the drop as it progressed down the linear part of the gradient. At each position, the angles on both sides of the drop were averaged. From the slope of the plot of the cosine of the average contact angle vs position, the value of d(cos θ)/dx was obtained.

Acknowledgment. We thank S. Garoff for his advice on the design of the vibration setup used in these studies and H. Caram for valuable discussions, especially on the subject of drop shape resonance. We also thank Lisa Toback for helping us to collect some of the data presented here. This work was supported by an unrestricted grant from DuPont via Polymer Interface Center, a laboratory renovation grant from Lehigh University, and the Office of Naval Research.

Note Added after ASAP Posting. This article was released ASAP on April 13, 2004. A sentence was changed in the first paragraph of the results and discussion section. The correct version was posted on April 20, 2004.

LA036221A